Highly time-resolved characterization of carbonaceous aerosols using a two-wavelength Sunset thermo/optical carbon analyzer

Mengying Bao[1,2,3], Yan-Lin Zhang[1,2,3*], Fang Cao[1,2,3], Yu-Chi Lin[1,2,3], Yuhang Wang[4], Xiaoyan Liu[1,2,3], Wenqi Zhang[1,2,3], Meiyi Fan[1,2,3], Feng Xie[1,2,3], Robert Cary[5], Joshua Dixon[5] and Lihua Zhou[6]

1 Yale-NUIST Center on Atmospheric Environment, Joint International Research Laboratory of Climate and Environment Change (ILCEC), Nanjing University of Information Science and Technology, Nanjing 210044, China

2 Key Laboratory of Meteorological Disaster Ministry of Education (KLME), Collaborative Innovation Center on Forecast and Evaluation of Meteorological Disasters (CIC-FEMD), Nanjing University of Information Science and Technology, Nanjing 210044, China

3 School of Applied Meteorology, Nanjing University of Information Science and Technology, Nanjing 210044, China

4 School of Earth and Atmospheric Sciences, Georgia Institute of Technology, Atlanta 30332, USA

5 Sunset Laboratory, 1080 SW Nimbus Avenue, Suite J/5 Tigard, OR 97223, USA

6 College of Global Change and Earth System Science, Beijing Normal University, Beijing 100875, China

Correspondence: Yan-Lin Zhang (dryanlinzhang@outlook.com)

Abstract

Carbonaceous aerosols have great influence on the air quality, human health and climate change. Except for organic carbon (OC) and elemental carbon (EC), brown carbon (BrC), mainly originates from biomass burning, as a group of OC with strong absorption from the visible to near-ultraviolet wavelengths, makes a considerable contribution to global warming. Large amounts of studies have reported long-term observation of OC and EC concentrations throughout the word, but studies of BrC based on long-term observations are rather limited. In this study, we established a two-wavelength method (658 nm and 405 nm) applied in the Sunset thermo/optical carbon analyzer. Based on one-year observation, we firstly investigated the characteristics, meteorological impact and transport process of OC and EC. Due to BrC absorbs light at 405 nm more effectively

than 658 nm, we defined the enhanced concentrations (dEC =$EC_{405\ nm}$—$EC_{658\ nm}$) and gave the possibility to provide an indicator of BrC. The receptor model and MODIS fire information were used to identify the presence of BrC aerosols. Our results showed that the carbonaceous aerosols concentrations were highest in winter and lowest in summer. Traffic emission was an important source of carbonaceous aerosols in Nanjing. Receptor model results showed that strong local emissions were found in OC and EC aerosols, however dEC aerosols were significantly affected by regional or long-range transport. The dEC/OC and OC/EC ratios showed similar diurnal patterns and the dEC/OC increased when the OC/EC ratios increased, indicating strong secondary sources or biomass burning contributions to dEC. Two biomass burning events both in summer and winter were analyzed and the results showed that the dEC concentrations were obvious higher in biomass burning days, however, no similar levels of the OC and EC concentrations were found both in biomass burning days and normal days in summer, suggesting that biomass burning emission made a great contribution to dEC and the sources of OC and EC were more complicated. Large number of open fire counts from the northwest and southwest areas of the study site were monitored in winter, significantly contributed to OC, EC and dEC. In addition, the near-by YRD area was one of the main potential source areas of dEC, suggesting that anthropogenic emissions could also be important sources of dEC. The results proved that dEC can be an indicator of BrC in biomass burning days. Our modified two-wavelength instrument provided more information than traditional single-wavelength thermo/optical carbon analyzer and gave a new idea about the measurement of BrC, the application of dEC data need to be further investigated.

1. Introduction

Carbonaceous aerosols including organic carbon (OC) and elemental carbon (EC), which have significant influence on the global radiative transfer, human health and atmospheric visibility, have been the focus of research in the atmospheric environment field for many years (Lelieveld et al., 2015; Wu and Yu, 2016; Wang et al., 2018; Zhang et al., 2017; Liu et al., 2019; Zhang et al., 2019). EC mainly originates from fossil fuel and biomass combustion and is estimated to be the second largest warming factor behind CO_2 contributing to climate change (Liu et al., 2015; Zhang and Kang, 2019; Cao and Zhang, 2015). OC originates both from primary emissions and gas-to-particle conversion as secondary organic carbon (SOC) and can scatter the solar radiation which causes negative forcing globally (Zhou et al., 2014; Huang et al., 2014).

In the recent decades, brown carbon (BrC), as a kind of light-absorbing organic carbon which can absorb light especially from near-UV to visible wavelength, has caused global concern due to its positive climate effect (Andreae and Gelencsér, 2006; Zhang et al., 2020). BrC is mainly emitted from anthropogenic and biogenic emissions (Zhang et al., 2011). Previous studies have proved that biomass burning and biofuel combustion are the most important sources of primary BrC (Saleh et al., 2014; Wu et al., 2020; Lei et al., 2018). Recent researches reported that in developing countries such as China and India, the contribution of fossil fuel combustion to BrC can't be ignored (Satish et al., 2017; Yan et al., 2017; Kirillova et al., 2014). Secondary BrC is mainly emitted from heterogeneous photo-oxidation reactions or aqueous reactions of anthropogenic and biogenic precursors (Zhang et al., 2020; Li et al., 2020; Zhang et al., 2011). However, due to the lack of understanding of BrC at the molecular level and in situ BrC data, there are still large uncertainties in the estimates of the distribution and the magnitude of BrC climate effect in both remote sensing and modeling method (Arola et al., 2011; Feng et al., 2013).

The thermo-optical analysis (TOA) method is one of the most widely used quantitative method of OC and EC taking use of the difference between the thermo-optical properties of OC and EC (Birch and Cary, 1996; Chow et al., 2004). OC and EC will be volatilized at different heating protocol. The reflectance/transmittance of one laser source (near-infrared wavelength) through the sample filter are continuously monitored and return of the reflectance/transmittance to its initial value on the thermograph was taken as a split point between OC and EC. This way, the formation of pyrolyzed carbon which can also absorb the light and make the sample darker, is corrected. This method has been wildly used in present studies applied in the NIOSH protocol or IMPROVE_A protocol (Ji et al., 2016; Chow et al., 2007). However, the thermo-optical approach assumed that EC is the only light-absorbing species, the presence of BrC, which is part of OC but also a light-absorbing component, shifts this separation towards EC, resulting in overestimated EC values and underestimated OC values (Chen et al., 2015; Birch and Cary, 1996).

Sandradewi et al. (2008) pointed out that light absorption measurements at different wavelength by the aethalometer can be used to quantify the contributions of wood combustion and traffic emissions to aerosols since wood smoke contains organic compounds which enhance the light absorption in ultraviolet wavelength. But traffic emissions produce more BC, which dominates the light absorption in near-infrared wavelength. They took use of aethalometer data measured at 470 nm and 950 nm to quantify the BC distinction between wood burning and traffic emission. With the

similar principle, Wang et al. (2011) used a two-wavelength Aethalometer (370 and 880 nm) to identify the presence of residential wood combustion (RWC) particles which was closely associated with BrC. Organic components of wood smoke particles absorb light at 370 nm more effectively than 880 nm in two-wavelength aethalometer measurements. They believed that the enhanced absorption (Delta-C=BC_{370nm}-BC_{880nm}) can serve as an indicator of RWC particles. This method was further used by Wang et al. (2012a) and Wang et al. (2012b). Chen et al. (2015) used a modified seven-wavelength TOT/TOR instrument (Thermal Spectral Analysis – TSA) allowing the determination of the OC-EC split at different wavelengths and light absorption measurements to be made with wavelength-specific loading corrections, providing additional information including the optical properties of black carbon (BC) and BrC from the IR to UV parts of the solar spectrum and their contributions. Massabò et al. (2016) further corrected the OC/EC split point using the Multi-Wavelength Absorbance Analyzer (MWAA) which provides the aerosol absorbance values at five wavelengths from IR to UV together with a Sunset OC/EC analyzer to achieve the BrC concentration. With a set of samples collected wintertime in the Ligurian Apennines in Italy, clear correlations were found between the BrC and levoglucosan mass concentration. A further step of BrC quantification taking use of TSA was reported by Chow et al. (2018), further proving that the use of seven wavelengths in thermal–optical carbon analysis allows contributions from biomass burning and secondary organic aerosols to be estimated. Their results clearly demonstrated the role of BrC in the thermo-optical analysis. However, these techniques focus on the light absorption measurement of BrC and are still limited reported in previous researches, though they provide quartz-fiber filter samples that are currently being characterized for organic carbon (OC) and EC by thermal/optical analysis. These methods mentioned above still can't achieve the observation of long-term real-time BrC mass concentrations.

Since the establishment of the thermal–optical transmittance (TOT) method by the Sunset Laboratory, the Sunset OC/EC instrument, as part of the Chemical Speciation Network (CSN), where cover over 100 monitors across the United States over 15 years, offering long-term measurement of OC and EC concentrations, has been widely used in the United States and throughout the world providing important in-situ data of OC and EC aerosols (U.S.EPA, 2019; Birch and Cary, 1996). This instrument had been designed with a tuned diode laser (red 660 nm) to correct the formation of pyrolyzed carbon. In this study, we modified the Sunset instrument to a two-wavelength (658 nm and 405 nm) Sunset carbon analyzer by adding one more violet diode

laser at λ=405 nm. The violet diode laser together with the red diode laser, focus through the sample chamber then the laser beam passed through the filter to correct for the pyrolysis-induced error. Previous work reported by Chen et al. (2015) as mentioned above was integrating the optical instrument like the aethalometer to the traditional OC/EC analyzer, in this way, they provided the light absorption contributions of BC and BrC. The enhanced carbon analyzer provided new insight into more accurate OC and EC measurements. Their work was conducted in offline mode, based on their work, our instrument can get the real-time OC and EC mass concentrations both at 658 nm and 405 nm. BrC particles absorb light at 405 nm more effectively than 658 nm in the two-wavelength Sunset carbon measurements. We define $dEC=EC_{405\ nm}-EC_{658\ nm}$ and hope it can be an indicator of BrC aerosols so that we can divide real-time BrC mass concentration measurement from the two-wavelength measurement.

Nanjing, as one of the largest cities in the Yangzi River Delta region, represents a heavy industry area with a dense population. In addition, due to its topography, Nanjing is very sensitive to regional transport of air masses from its surrounding areas. OC, EC and dEC aerosols were observed from June 2015 to July 2016 at Nanjing University of Information Science and Technology (NUIST). Based on the abundant data, together with MODIS fire information, we can analyze the temporal variation, transport processes and sources of carbonaceous aerosols in North Nanjing and evaluate the biomass burning impact on dEC aerosols, which can be the scientific basis of pollution control policy.

2. Methods

2.1 Study site

In this study, the sampling site is located at Nanjing University of Information Science and Technology (NUIST) in the North Suburb of Nanjing (32°207′N, 118°717′E). The study site is surrounded by housing and industrial areas. Many chemical enterprises, for example, Yangzi Petrochemical, Nanjing Chemical Industry and Nanjing Iron and Steel Group are located at the northeast of the study region, which produces exhaust with large amounts of aerosol particles. The study site is adjacent to a heavily trafficked road (Ningliu Road) located near the site, approximately 600 m to the east. Therefore, this region has intense human activities, industrial emissions and heavy traffic flow.

2.2 Two-wavelength TOT measurement

Hourly concentrations of OC and EC in $PM_{2.5}$ were sampled and measured by a semi-

continuous carbon analyzer (Model-4, Sunset Lab, USA). Air samples were collected continuously with a sample flow of ~8 L/min through a $PM_{2.5}$ cyclone. The collection time was set at 45 min for each cycle. The airstream passed through a parallel plate organic denuder to reduce the effect of volatile organic compounds and finally deposited on a quartz filter with a diameter of ~17mm.

After a sample was collected, OC and EC were analyzed using the thermal-optical transmittance (TOT) method and applied a slightly modified NIOSH 5040 protocol. The details of the heating setup were shown in Table S1. Figure 1 shows the structure and operational principle of the instrument. Briefly, it consists of two-stages: the oven was first purged with helium and the oven temperature increased in a stepped ramp to 840℃, OC was volatilized in this stage. Then the oven temperature kept at 840℃ for a while and went down to 550℃. In the second stage, EC was volatilized in a second temperature ramp to 850℃ while purging the oven with a mixture containing 2%oxygen and 98%helium. The pyrolysis products were converted to carbon dioxide (CO_2) which was quantified using a self-contained nondispersive infrared (NDIR) system.

Also, in this study, we used two-diode lasers (658nm and 405nm) equipped Sunset analyzer, thus mass concentrations of OC and EC at different wavelengths can be measured with the 2-lasers system. The split point between OC and EC was detected automatically by the RTCalc731 software provided by Sunset Lab. The principle was same as the traditional Sunset carbon analyzer (Birch and Cary, 1996). An example thermogram of sample analysis using the two-wavelength Sunset semi-continuous carbon analyzer was shown in Fig. 2. During the sample analysis, the laser beam at 658 nm and 405 nm were both sent through the filter and the transmitted light signal were monitored to correct the undesired formation of pyrolyzed carbon (PyrC) and then to determine the split point of OC and EC at both two wavelengths. BrC aerosols absorb light at 405nm more significantly than 658nm in the 2-lasers system. Due to the strong absorption of BrC in near-ultraviolet wavelength, thus this enhanced absorption at 405nm can serve as an indicator of BrC aerosols (Liu et al., 2015). We define dEC data as the difference of EC concentrations at two wavelengths ($dEC=EC_{405nm}-EC_{658nm}$) to identify the presence of BrC aerosols. Our study provided a one-year measurement of dEC mass concentrations. Besides, OC and EC represent the OC and EC concentrations at 658nm in this paper without a special explanation.

At the end of each analysis, a fixed volume of an internal standard containing 5%methane and 95%Helium was injected and thus a known carbon mass could be derived. The external sucrose standard (4.207 $\mu g\ \mu L^{-1}$) calibration was conducted every week to insure repeatable quantification.

Calibration with an instrument blank was conducted every day. Both detection limit for OC and EC of the instrument was 0.5 μg m^{-3}. We also did the measurements of OC and EC in $PM_{2.5}$ filter samples using the same method followed by the NIOSH protocol. All the data were corrected to blank measurement before comparison. Figure S1 shows the correlations between the real-time OC, EC concentrations and sampling OC, EC concentrations at the same time. The results showed that the online and offline data during the corresponding periods had good correlations with R^2 of 0.8 for OC, $R^2$of 0.4 for EC and R^2 of 0.8 for TC. In order to evaluate the impact of PyrC, we calculated the PyrC at 658 nm fraction of dEC and the average PyrC/dEC was 4.4%, indicating the little influence of PyrC.

2.3 Test of the new dEC data

To evaluate the new dEC data, parallel BC concentrations were measured with a seven-wavelength Aethalometer with dEC concentrations in December, 2019. Radiation attenuation of an aerosol deposition on a filter (ATN_λ) is determined by the Beer-Lambert law:

$$ATN_\lambda = ln\frac{I_{0,\lambda}}{I_\lambda} \quad \text{Equation. (1)}$$

Where $I_{0,\lambda}$ and I_λ were the measured wavelength-specific laser reflectance signals. ATN_λ is used to calculate the attenuation coefficient with Eq. (2):

$$b_{ATN} = \frac{A}{V} \quad \text{Equation. (2)}$$

Where A was the filter area and V is the sampled air volume. Then a simplified two-component model was used to calculate the contribution of light attenuation to both BC and BrC (Chow et al., 2018;Chen et al., 2015;Sandradewi et al., 2008;Hareley et al., 2008):

$$b_{ATN}(\lambda) = q_{BC} \times \lambda^{-AAE_{BC}} + q_{BrC} \times \lambda^{-AAE_{BrC}} \quad \text{Equation. (3)}$$

Where q_{BC} and q_{BrC} were fitting coefficients, AAE was the absorption Ångström exponent which represented the wavelength-dependent characteristics of light absorption capability of aerosols. The AAE of BC was assumed to be 1. Fitting coefficients in Eq. (3) were obtained for potential AAE_{BrC} between 1 and 8 by least square linear regression and the AAE_{BrC} led to the overall best fit in terms of r^2 is selected as the effective AAE_{BrC}. Using these fitting coefficients, the b_{ATN} due to BC and BrC are calculated at each wavelength. Figure S2 showed that the fitted b_{ATN} at 405 nm were within ±5 % of the measured values for $b_{ATN} > 0.01$. Figure 3 showed the relationship between the b_{ATN} due to BrC at 405 nm and the dEC. Good correlation between them were found with R square of 0.64, indicating that dEC was associated with BrC.

2.4 Sampling

2.4.1 Real-time $PM_{2.5}$ observation

The real-time $PM_{2.5}$ concentrations were measured through the Tapered Element Oscillating Microbalance (TEOM) method (TEOM1405-DF, Thermo Scientific, America) from August, 2015 to July, 2016. The resolution of the measured data was 6 min. The instrumental operation maintenance, data assurance and quality control were performed according to the Chinese Ministry of Environmental Protection Standards for PM_{10} and $PM_{2.5}$ which was named "HJ 653-2013" (Zhang and Cao, 2015b).

2.4.2 Sample collections

$PM_{2.5}$ in the atmosphere were collected on prebaked quartz fiber filters which were under 450℃ for 6 hours (QFF, PALL, America) with 8*10 inch by a high volume air sampler (KC-1000, Qingdao, China) at a flow rate of 999 L min^{-1} in four months: 4 June to 18 June, 6 October to 2 November and 10 December to 31 December in 2015, 10 May to 31 May in 2016. Sampling started and ended at around 8:00 and 20:00 every day; each sample was collected for 12 hours. A total of 148 samples were collected including four field bank filters in four seasons collected following 10 mins exposures to ambient air without active sampling.

All QFFs were pre-baked at 450 °C for 6 h before sampling to remove residual carbon. Before and after sampling, all QFFs were weighed by electronic balance (Sartorius, 0.1 mg, Germany). After weighting, the filters were wrapped in aluminum foils, packed in air-tight polyethylene bags and stored at -20˚C for further analysis. All procedures during handling of filters were strictly quality controlled to avoid any possible contamination.

2.5 Identification of potential regional sources

The Hybrid Single-Particle Lagrangian Integrated Trajectory (HYSLPIT4.8) model, provided by the National Oceanic and Atmospheric Administration (NOAA) were used to investigate the air mass origins of carbonaceous aerosols. The 48-hour back trajectories at Nanjing (32.2°N, 118.7°E) were calculated every hour (Draxler and Hess, 1998;Rolph et al., 2017;Cohen et al., 2015). In order to evaluate the behavior of the air masses circulation in the planetary boundary layer (PBL), the trajectories at 500m corresponding to the upper-middle height of the PBL were calculated, representing well-mixed convective boundary layer for regional transport investigation (Xu and Akhtar, 2010). The National Center for Environmental Prediction Global Data Assimilation System (NCEP GDAS) data obtained from NOAA with a spatial resolution of 1° ×1°

247 and 24 levels of the vertical resolution were used as meteorological data input to the model. The
248 Potential Source Contribution Function (PSCF) model was usually applied to localize the potential
249 sources of pollutants. The details about the setup of the model can be seen in the research reported
250 by Bao et al. (2017).

251 **3. Results and discussion**

252 **3.1 Characteristics of carbonaceous aerosols**

253 3.1.1 Concentrations of carbonaceous aerosols

254 The statistics for the $PM_{2.5}$, OC, EC and dEC mass concentrations at the NUIST site are
255 summarized in Table 1. The hourly OC concentrations ranged from 0.5 to 45.8 μg m^{-3} (average of
256 8.9 ± 5.5 μg m^{-3}), and the EC concentrations ranged from 0.0 to 17.6 μg m^{-3} (average of 3.1 ± 2.0
257 μg m^{-3}). The results were comparable to those reported by Chen et al. (2017) in the Xianlin Campus
258 of Nanjing University (5.7 μg m^{-3} for OC and 3.2 μg m^{-3} for EC), which site was located in the
259 southeast suburb of Nanjing and close to the G25 highway and were also affected by traffic sources.
260 The higher OC concentrations in this study were probably due to the around chemical enterprise
261 emissions. The average contributions of OC and EC to the total measured $PM_{2.5}$ mass was 12.8%
262 and 4.3%, respectively, suggesting that carbonaceous fraction made an important contribution to
263 fine particulate matter. The average dEC mass concentration was 0.8 μg m^{-3} contributing 10.0% to
264 OC, 22.3% to EC and 1.3% to $PM_{2.5}$ concentrations with max concentration of 8.1 μg m^{-3}
265 contributing 48.2% to OC, 97.8% to EC and 17.6% to total $PM_{2.5}$ concentrations. This information
266 can be further applied in the PMF analysis to evaluate the sources of carbonaceous aerosols (Zhu
267 et al., 2014;Sahu et al., 2011;Yan et al., 2019).

268 Compared with carbonaceous aerosols levels in other cities (Table S2), the OC and EC
269 concentrations in Nanjing were generally lower than those observed in urban sites such as Beijing
270 and Shanghai and inland cities like Chengdu and Chongqing which was affected by the basin
271 terrain characteristics with static wind and unfavorable diffusion conditions, but higher than those
272 observed in the southern coastal cities such as Guangzhou, which was a megacity in China. It could
273 be explained since the site set in Guangzhou was a rural site. In general, the level of carbonaceous
274 aerosols concentrations in China was higher than that in developed countries in the United States
275 and Europe and lower than that in developing countries like India, though the sampling period in
276 India was from late autumn to winter, the much higher concentrations in India indicated the heavy
277 pollution level. The average OC/EC ratios in this study was 3.6, which was lower than most of

those reported in other studies, indicating the important impact of vehicle emissions in our study site.

Figure 4 shows the mass fractions of hourly carbonaceous aerosols and OC/EC ratios at different $PM_{2.5}$ concentration intervals during the study periods. During the study period, 84.2% of the $PM_{2.5}$ samples exceeded the daily averaged Chinese national ambient air quality standard (NAAQS) of 35.0 μg m^{-3} for the first grade and 40.1% of the total samples exceeded the NAAQS of 75.0 μg m^{-3} for the second grade, reflecting heavy aerosol pollution in the study area. Generally, the fractions of carbonaceous components decreased with increasing $PM_{2.5}$ pollution level. Larger mass fraction (about 32.3%) of carbonaceous aerosols in $PM_{2.5}$ was found for period relatively lower $PM_{2.5}$ levels (0–20 μg m^{-3}) compared to high $PM_{2.5}$ levels (300–500 μg m^{-3}) with carbonaceous aerosols mass fraction of 5.2%. The result indicated other components like secondary inorganic aerosol (SIA) contributes more significantly to heavy haze events in Nanjing, which was also found in other cities in the Yangtze River Delta area (Yang et al., 2011; Zhang and Zhang, 2019). The contribution of dEC to OC decreased with the increase of $PM_{2.5}$ concentrations between 0-200 μg m^{-3}, and then increased with the increase of $PM_{2.5}$ concentrations between 200-500 μg m^{-3}. The dEC contributed most significantly to OC of 14.3% when $PM_{2.5}$ concentrations below 20 μg m^{-3}. Similar trend was found in OC/EC ratios which showed a sharp increase along with enhanced $PM_{2.5}$ level above 150 μg m^{-3}. Previous studies had reported that high OC/EC ratios were related to SOC formation or biomass burning emissions whereas low OC/EC ratios were related to vehicle exhaust (Wang et al., 2015). We divided the dEC/OC at different intervals of OC/EC ratios and found that the dEC/OC increased when the OC/EC ratios increased in four seasons, indicating strong secondary sources or biomass burning contributions to dEC during heavy pollution periods (Fig. S3).

3.1.2 Seasonal variations of carbonaceous aerosols

As shown in Fig. 5, the OC, EC, dEC concentrations and dEC/OC ratios showed similar variations with highest in winter and lowest in summer. The average OC and EC concentration in winter was ~1.4 times and 1.5 times higher than that in summer and the average dEC concentrations and dEC/OC in winter were approximately 1.4 and 1.6 times higher than those in summer (Table 1). High dEC/OC was found in January and February in winter, indicating strong influence of anthropogenic sources on dEC, such as coal combustion. In addition, we found strong biomass burning activities in February, which significantly contributed to the high concentrations

of dEC in February, more details could be found in section 3.3. The seasonality of carbonaceous species in $PM_{2.5}$ was strongly influenced by seasonal variations in emissions intensities and meteorological parameters. Table S3 summarizes the meteorological parameters in four seasons during the study period. The high carbonaceous aerosols concentrations in winter were mainly a result of relatively stable atmospheric conditions with low temperature, relative humidity and boundary layer on one hand, and on the other hand, increasing emissions from fossil-fuel combustion for heating from the chemical enterprises nearby. In summer, higher boundary layer resulted in the dispersion of aerosols in the atmosphere, and higher temperature promoted the partitioning of semi-volatile organic compounds (SVOCs) into gaseous phase (Yang et al., 2011). In addition, large precipitation in summer (586 mm in total) favored the wet scavenging processes of aerosols.

The OC/EC ratios in spring, summer, autumn and winter were 3.9, 4.0, 2.8 and 3.4, respectively (Table 1). The OC/EC ratio could give some information about primary and secondary organic carbon (Turpin and Huntzicker, 1995; Lim and Turpin, 2002). In summer, strong convective activities in the atmospheric boundary layer and solar radiation, high temperature and plenty of moisture in the atmosphere were favorable for the formation of SOC. On the other hand, the high OC/EC ratios in June in this study were also strongly related to biomass burning which will be discussed in the 3.3 sections. The lower ratios of OC to EC in autumn and winter indicated that strong primary sources in these two seasons. It should be noted that the OC/EC ratios were a rough indicator to estimate the primary and secondary organic carbon, further analysis of the formation of SOC need to be conducted in the future (Pio et al., 2011;Wu and Yu, 2016).

3.1.3 Diurnal variation of carbonaceous aerosols

The diurnal pattern of carbonaceous aerosols can be affected by both meteorological parameters and sources (Ji et al., 2016). Figure 6 depicts the diurnal variation of OC, EC, dEC, dEC/OC and OC/EC ratios during the study period. Clear diurnal variations were observed in OC and EC aerosols. Both the OC and EC concentrations kept high levels at night and low levels in the daytime, indicating the strong influence of the atmospheric boundary layer on air quality in the northern Nanjing. The peak occurred in the morning both in OC and EC indicating the significant impact of traffic source on the OC and EC concentrations. The dEC/OC and OC/EC ratios showed similar trends in the daytime with gradually increase from morning till afternoon, indicating the importance of the contribution of secondary sources to dEC. Similar though not so obvious diurnal

variations were found in dEC. It should be noted that the vehicle emissions and the boundary layer height had no significant effect on the diurnal variation of dEC/OC, suggesting there was no significant local sources of dEC. There was a small peak in dEC/OC at 3:00 am, which might be related to the aqueous secondary organic aerosols formations during nighttime (Sullivan et al., 2016).

The relative humidity (RH) and Temperature (T) dependent distributions of OC, EC mass concentrations and dEC/OC and OC/EC throughout the study period are shown in Fig. 7. High dEC/OC (>30 %) could be found in three areas, first showed in the right area with relatively high T at 25-40 ℃ and RH at 40-60 %, which were usually found in the summer afternoon which was closely related to the strong formation of SOC. This distribution was also shown in OC/EC. The second area was displayed in the upper region with RH over 80 % and T at 10-20 ℃ and the third area appeared when RH below 30 % and T at about 10 ℃, corresponding to nighttime and winter afternoon. In general, dEC had no strong dependence on the RH and T distribution, indicating the complex formation mechanism of dEC. The OC and EC showed similar distributions with the highest mass loading (OC: > 20 μg m^{-3}; EC: > 8 μg m^{-3}) at relatively high RH at 60-80 % which usually occurred at night with relatively low boundary layer height, leading to the accumulation of aerosols. However the corresponding OC/EC ratios were low, suggesting the importance of primary sources to OC and EC in northern Nanjing, which will be verified in the wind rose of OC and EC (Fig. 8).

3.2 Air mass transport

3.2.1 Windrose of carbonaceous aerosols

To investigate the influences of air masses transport to the study site, the wind rose of OC, EC and dEC/OC using hourly data in four seasons is illustrated in Fig. 8 (Carslaw and Ropkins, 2012). Two points should be noted. First, high OC and EC mass concentrations were found near the field site (indicating by WS < 1 m s^{-1}), suggesting that local and primary emissions (e.g., industrial and vehicle emissions) were stable and important sources contributing to atmospheric OC and EC mass concentrations in northern Nanjing. The OC mass concentrations from the southwest increased with the increase of WS in summer, indicating that sources of OC are complicated in summer including secondary reaction during long-range or regional transport. Second, compared with OC and EC, dEC aerosols showed no significant local sources. The dEC/OC increased with the increasing of WS and highest dEC/OC were found when WS over 3 m s^{-1}. Long-range or regional

transport was highly likely the main sources contributing to dEC mass concentrations.

3.2.2 The potential source areas of carbonaceous aerosols

The possible source contributions were evaluated using the PSCF model and the PSCF map are shown in Fig. 9 (Petit et al., 2017). The areas with high PSCF values were highly likely the potential pollution source areas. As shown in Fig. 9, PSCF results further proved the strong regional transport contribution to dEC aerosols and local contributions to OC and EC aerosols. In spring, the potential source areas of OC and EC were mainly from the southwest of Nanjing, however, the potential source areas of dEC aerosols were from the east of Nanjing, indicating obvious different sources between OC, EC and dEC. In summer, local areas were the main sources areas of EC and the near-by Yangtze River Delta City Group from southeast of Nanjing including developed cities like Shanghai were the main sources areas of OC and dEC. The anthropogenic emissions from these areas might be important sources of OC and dEC. Besides, both the potential sources areas of dEC and EC were displayed in the northwest of Nanjing in summer, suggesting strong primary sources of dEC from this area which were very likely associated to biomass burning, more details were in the section 3.3. In autumn, strongest local sources from the study site of OC and EC were found. However the dEC mainly originated from regional transport from the northwest and southeast areas of Nanjing. Biomass burning has been proved to be an important source of air pollutants in the Yangtze River Delta (YRD) area, especially in the wheat harvest seasons (e.g., June and October) (Cheng et al., 2014; Zhang and Cao, 2015a). In addition, the YRD area is the most economically developed region in China and has lots of industrial cities, which means that industrial emissions and anthropogenic sources contributed to high carbonaceous aerosols pollution levels. In winter, dEC were mainly from long-range transport from northern cities and regional transport from the southwest areas of Nanjing while both long-range transport and local sources were found in OC and EC concentrations.

3.3 The characteristics of carbonaceous aerosols during biomass burning periods

The biomass burning emission has been proved to be an important source of BrC on a global scale, it is consistently observed in large-scale forest fire events (Laskin et al., 2015). Based on the Fire Information for Resource Management System (FIRMS) derived from the Moderate Resolution Imaging Spectroradiometer (MODIS), we found that the fire points reached to 2028, 1773 and 967 on 11 Jun 2015, 7 February 2016 and 2 Mar 2016 in the areas around our study site, respectively, suggesting there were strong biomass burning events on these days (Fig. S4). To

further investigate the biomass burning impact on dEC aerosols, we analyzed the temporal trends of carbonaceous aerosols from 4 June 2015 to 19 June 2015 and 7 February 2016 to 3 Mar 2016, respectively. Combining the observed aerosols concentrations and fire information, we divided the periods into normal days and biomass burning days. It should be noted that the biomass burning days are not determined based only on fire points. We also considered the 48-h backward trajectories and open biomass burning areas. For example, we did found lots of fire points from 11 June 2015 to 12 June 2015 and from 7 February 2016 to 10 February 2016, respectively, and the 48-h back trajectories went through these biomass burning areas (Fig. S5b, c). However, although there were large amounts of fire points in northwest of Nanjing from 8 June 2015 to 9 June 2015, the backward trajectory showed air mass during the periods came from the southeast areas where no open fire points were found (Fig. S5a). In contrast, there were only a few fire points found near the study site from 26 February 2016 to 27 February 2016, the 48-h backward trajectory showed the air mass was exactly from the area (Fig. S5d).

As shown in Fig. 10 and Fig. 11, we found that dEC concentrations, dEC/OC and OC/EC ratios showed peaks during each biomass burning periods which was not that obvious in OC and EC concentrations, suggesting the unique biomass burning impact on dEC and the sources of OC and EC were more complicated. It should be noted that there were peaks of dEC appeared on 9 June 2015 and 13 February 2016, which were not biomass burning days, suggesting that biomass burning was not the only sources of dEC. As mentioned in the 3.1 and 3.2 section, anthropogenic emissions could be the sources of dEC and the secondary sources couldn't be ignored, too. Summarized in Table 2 are the average and standard deviation values of OC, EC, OC/EC, dEC and dEC/OC during biomass burning and normal days. The OC/EC, dEC concentrations and dEC/OC were obvious higher in biomass burning days than those in normal days, but similar levels of the OC and EC concentrations were found both in biomass burning days and normal days in summer, suggesting the great contribution of biomass burning emissions to dEC aerosols and there were other sources of OC and EC in summer. All the carbonaceous aerosols were higher in biomass burning days in winter, in addition, the location of open fire counts were mainly in the northwest and southwest area of the study site (Fig. S5c, d), which were the potential source areas of OC, EC and dEC in winter as discussed in the section 3.2.2, indicating strong contributions of biomass burning emissions to all the carbonaceous aerosols in winter.

4. Conclusion

In this study, the characteristics and sources of carbonaceous aerosols in North Nanjing were investigated and we introduced a two-wavelength method by modifying the Sunset carbon analyzer. We incorporated a new diode laser at λ=405 nm in the instrument, making it possible to detect the laser beam passing through the filter at both wavelength at λ=658 nm and λ=405 nm, so we can obtain the dEC concentrations. Our study illustrated the feasibility of using dEC to characterize the BrC aerosols, providing a new idea about the measurement of BrC. The results showed that high (low) OC, EC and dEC concentrations were found in Winter (summer), indicating the significant impact of the increase of various emission sources in winter and wet scavenging of rain in summer. Similar diurnal cycles for OC and EC concentrations were found with high at night and low in daytime, strongly affected by the boundary layers. Traffic emissions were found to have significant influence on the concentrations of OC and EC. Similar trends were found in the diurnal cycle of dEC/OC and OC/EC and the dEC/OC increased when the OC/EC ratios increased, indicating strong secondary sources or biomass burning impact on dEC. The wind rose and receptor model results showed that strong local emissions were found in OC and EC aerosols, however dEC aerosols were significantly affected by regional or long-range transport. The near-by YRD area was one of the main potential source areas of dEC, suggesting that anthropogenic emissions could be the sources of dEC. Together with the back trajectories analysis and MODIS fire informations, we analyzed two biomass burning events both in summer and winter. The results showed that the sources of OC and EC were more complicated than those of dEC aerosols in summer. Biomass burning emission made a great contribution to dEC concentrations in summer. Large number of open fire counts from the northwest and southwest areas of the study site were monitored, significantly contributed to all the carbonaceous aerosols pollutions in winter.

Our modified two-wavelength instrument provided more information than traditional single-wavelength thermo/optical carbon analyzer. The results proved that dEC can be an indicator of BrC in biomass burning days. It should be noted that the sources of dEC were complicated and the anthropogenic emissions and secondary formations of dEC aerosols couldn't be ignored , further chemical analysis need to be conducted in the future. The evaluation of SOC formation and the relationship between dEC and SOC can be conducted. In addition, More chemical analysis such as the analysis of the ion, the organic matter or the sugars in $PM_{2.5}$ can be measured, thus we can get some information of the tracers of different sources and more accurate and quantitative source apportionment can be done (Bhattaraia et al., 2019;Wu et al., 2018;Wu et al., 2019). We also hope

that the dEC data can be further applied in more researches.

Acknowledgments

This research is financially supported by the National Natural Science Foundation of China (grant no. 41977305), the Provincial Natural Science Foundation of Jiangsu (grant no. BK20180040) and the Postgraduate Research & Practice Innovation Program of Jiangsu Province (grant no. KYCX18_1014). This study is supported by the funding of Jiangsu Innovation & Entrepreneurship Team. The authors would also like to thank the China Scholarship Council for the support to Mengying Bao.We would also like to express our gratitude to Yuanyuan Zhang, Zufei Xu and Tianran Zhang for their assistance in the instrument maintenance throughout the obsevation period. Besides, we are grateful for Prof. Yunhua Chang, who makes considerable comments and suggerestions to this paper.

References:

Andreae, M. O. and Gelencsér, A.: Black carbon or brown carbon? The nature of light-absorbing carbonaceous aerosols, Atmos. Chem. Phys., 6, 3131–3148, 2006.

Arola, A., Schuster, G., Myhre, G., Kazadzis, S., Dey, S., and Tripathi, S. N.: Inferring absorbing organic carbon content from AERONET data, Atmos. Chem. Phys., 11, 215-225, 10.5194/acp-11-215-2011, 2011.

Bao, M., Cao, F., Chang, Y., Zhang, Y.-L., Gao, Y., Liu, X., Zhang, Y., Zhang, W., Tang, T., Xu, Z., Liu, S., Lee, X., Li, J., and Zhang, G.: Characteristics and origins of air pollutants and carbonaceous aerosols during wintertime haze episodes at a rural site in the Yangtze River Delta, China, Atmos. Pollut. Res., 8, 900-911, 10.1016/j.apr.2017.03.001, 2017.

Bhattaraia, H., Saikawac, E., Wana, X., Zhue, H., Ram, K., Gao, S., Kang, S., Zhanga, Q., Zhang, Y., Wu, G., Wang, X., Kawamura, K., Fui, P., and Cong, Z.: Levoglucosan as a tracer of biomass burning recent progress and perspectives, Atmos. Res., 220, 20-33, 10.1016/j.atmosres.2019.01.004, 2019.

Birch, M. E. and Cary, R. A.: Elemental carbon-based method for occupational monitoring of particulate diesel exhaust: methodology and exposure issues, Analyst, 121, 1183-1190, 1996.

Carslaw, D. C., and Ropkins, K.: openair — An R package for air quality data analysis, Environ. Model. Softw., 27-28, 52-61, 10.1016/j.envsoft.2011.09.008, 2012.

Cao, F. and Zhang, Y.-L.: Principle, method development and application of radiocarbon (^{14}C) —based source apportionment of carbonaceous aerosols: a review, Adv. Earth Sci., 30, 425-432, 10.11867 / j. issn. 1001-8166. 2015. 04. 0425., 2015.

Chen, L. W. A., Chow, J. C., Wang, X. L., Robles, J. A., Sumlin, B. J., Lowenthal, D. H., Zimmermann, R., and Watson, J. G.: Multi-wavelength optical measurement to enhance thermal/optical analysis for carbonaceous aerosol, Atmos. Meas. Tech., 8, 451-461, 10.5194/amt-8-451-2015, 2015.

Cheng, Z., Wang, S., Fu, X., Watson, J. G., Jiang, J., Fu, Q., Chen, C., Xu, B., Yu, J., Chow, J. C., and Hao, J.: Impact of biomass burning on haze pollution in the Yangtze River delta, China: a case study in summer 2011, Atmos. Chem. Phys., 14, 4573-4585, 10.5194/acp-14-4573-2014, 2014.

Chow, J. C., Watson, J. G., Chen, L.-W. A., Arnott, W. P., Moosmüller, H., and Fung, K.: Equivalence of elemental carbon by thermal/optical reflectance and transmittance with different temperature protocols, Envirn. Sci. Technol., 38, 4414-4422, 10.1021/es034936u 2004.

Chow, J. C., Watson, J. G., Chen, L. W., Chang, M. C., Robinson, N. F., Trimble, D., and Kohl, S.: The IMPROVE_A temperature protocol for thermal/optical carbon analysis: maintaining consistency with a long-term database, J. Air. Waste. Manag. Assoc., 57, 1014-1023, 10.3155/1047-3289.57.9.1014, 2007.

Chow, J. C., Watson, J. G., Green, M. C., Wang, X., Chen, L. A., Trimble, D. L., Cropper, P. M., Kohl, S. D., and Gronstal, S. B.: Separation of brown carbon from black carbon for IMPROVE and Chemical Speciation Network $PM_{2.5}$ samples, J. Air Waste Manag. Assoc., 68, 494-510, 10.1080/10962247, 2018

Cohen, M. D., Stunder, B. J. B., Rolph, G. D., Draxler, R. R., Stein, A. F., and Ngan, F.: NOAA's HYSPLIT Atmospheric Transport and Dispersion Modeling System, B. Am. Meteorol. Soc., 96, 2059-2077, 10.1175/bams-d-14-00110.1, 2015.

Draxler, R. R., and Hess, G. D.: An overview of the HYSPLIT_4 modelling system for trajectories, dispersion, and deposition, Aust. Meteorol. Mag., 47, 295-308, 1998.

Feng, Y., Ramanathan, V., and Kotamarthi, V. R.: Brown carbon: a significant atmospheric absorber of solar radiation?, Atmos. Chem. Phys., 13, 8607-8621, 10.5194/acp-13-8607-2013, 2013.

Hareley, O. L., Corrigan, C. E., and Kirchstetter, T. W.: Modified Thermal-Optical Analysis Using Spectral Absorption Selectivity To Distinguish Black Carbon from Pyrolized Organic Carbon,

Envirn. Sci. Technol., 42, 8459–8464, 10.1021/es800448n, 2008.

Huang, R. J., Zhang, Y., Bozzetti, C., Ho, K. F., Cao, J. J., Han, Y., Daellenbach, K. R., Slowik, J. G., Platt, S. M., Canonaco, F., Zotter, P., Wolf, R., Pieber, S. M., Bruns, E. A., Crippa, M., Ciarelli, G., Piazzalunga, A., Schwikowski, M., Abbaszade, G., Schnelle-Kreis, J., Zimmermann, R., An, Z., Szidat, S., Baltensperger, U., El Haddad, I., and Prevot, A. S.: High secondary aerosol contribution to particulate pollution during haze events in China, Nature, 514, 218-222, 10.1038/nature13774, 2014.

Ji, D., Zhang, J., He, J., Wang, X., BoPanga, Liua, Z., Wang, L., and Wang, Y.: Characteristics of atmospheric organic and elemental carbon aerosols in urban Beijing, China, Atmos. Environ., 293-306, 10.1016/j.atmosenv.2015.11.020, 2016.

Kirillova, E. N., Andersson, A., Han, J., Lee, M., and Gustafsson, O.: Sources and light absorption of water-soluble organic carbon aerosols in the outflow from northern China, Atmos. Chem. Phys., 14, 1413-1422, 10.5194/acp-14-1413-2014, 2014.

Laskin, A., Laskin, J., and Nizkorodov, S. A.: Chemistry of atmospheric brown carbon, Chemical Reviews, 115, 4335-4382, 10.1021/cr5006167, 2015.

Lei, Y., Shen, Z., Zhang, T., Zhang, Q., Wang, Q., Sun, J., Gong, X., Cao, J., Xu, H., Liu, S., and Yang, L.: Optical source profiles of brown carbon in size-resolved particulate matter from typical domestic biofuel burning over Guanzhong Plain, China, Sci. Total. Environ., 622-623, 244-251, 10.1016/j.scitotenv.2017.11.353, 2018.

Lelieveld, J., Evans, J. S., Fnais, M., Giannadaki, D., and Pozzer, A.: The contribution of outdoor air pollution sources to premature mortality on a global scale, Nature, 525, 367-371, 10.1038/nature15371, 2015.

Li, C., He, Q., Hettiyadura, A. P. S., Kafer, U., Shmul, G., Meidan, D., Zimmermann, R., Brown, S. S., George, C., Laskin, A., and Rudich, Y.: Formation of secondary brown carbon in biomass burning aerosol proxies through NO_3 radical reactions, Environ. Sci. Technol., 54, 1395-1405, 10.1021/acs.est.9b05641, 2020.

Lim, H.-J. and Turpin, B. J.: Origins of primary and secondary organic aerosol in Atlanta: results of time-resolved measurements during the Atlanta supersite experiment, Environ. Sci. Technol., 36, 4489-4496, 10.1021/es0206487 2002.

Liu, S., Aiken, A. C., Gorkowski, K., Dubey, M. K., Cappa, C. D., Williams, L. R., Herndon, S. C., Massoli, P., Fortner, E. C., Chhabra, P. S., Brooks, W. A., Onasch, T. B., Jayne, J. T., Worsnop,

D. R., China, S., Sharma, N., Mazzoleni, C., Xu, L., Ng, N. L., Liu, D., Allan, J. D., Lee, J. D., Fleming, Z. L., Mohr, C., Zotter, P., Szidat, S., and Prevot, A. S. H.: Enhanced light absorption by mixed source black and brown carbon particles in UK winter, Nat. Commun., 6, 8435, 10.1038/ncomms9435, 2015.

Liu, X., Zhang, Y.-L., Peng, Y., Xu, L., Zhu, C., Cao, F., Zhai, X., Haque, M. M., Yang, C., Chang, Y., Huang, T., Xu, Z., Bao, M., Zhang, W., Fan, M., and Lee, X.: Chemical and optical properties of carbonaceous aerosols in Nanjing, eastern China: regionally transported biomass burning contribution, Atmos. Chem. Phys., 19, 11213-11233, 10.5194/acp-19-11213-2019, 2019.

Massabò, D., Caponi, L., Bove, M. C., and Prati, P.: Brown carbon and thermal–optical analysis: A correction based on optical multi-wavelength apportionment of atmospheric aerosols, Atmos. Environ., 125, 119-125, 10.1016/j.atmosenv.2015.11.011, 2016.

Pio, C., Cerqueira, M., Harrison, R. M., Nunes, T., Mirante, F., Alves, C., Oliveira, C., Sanchez de la Campa, A., Artíñano, B., and Matos, M.: OC/EC ratio observations in Europe: Re-thinking the approach for apportionment between primary and secondary organic carbon, Atmos. Environ., 45, 6121-6132, 10.1016/j.atmosenv.2011.08.045, 2011.

Petit, J. E., Favez, O., Albinet, A., and Canonaco, F.: A user-friendly tool for comprehensive evaluation of the geographical origins of atmospheric pollution: Wind and trajectory analyses, Environ. Model. Softw., 88, 183-187, 10.1016/j.envsoft.2016.11.022, 2017.

Rolph, G., Stein, A., and Stunder, B.: Real-time Environmental Applications and Display sYstem: READY, Environ. Model. Softw., 95, 210-228, 10.1016/j.envsoft.2017.06.025, 2017.

Sahu, M., Hu, S., Ryan, P. H., Le Masters, G., Grinshpun, S. A., Chow, J. C., and Biswas, P.: Chemical compositions and source identification of $PM_{2.5}$ aerosols for estimation of a diesel source surrogate, Sci. Total. Environ., 409, 2642-2651, 10.1016/j.scitotenv.2011.03.032, 2011.

Sandradewi, J., Prévôt, A. S. H., Szidat, S., Perron, N., Alfarra, M. R., Lanz, V. A., Weingartner, E., and Baltensperger, U.: Using Aerosol Light Absorption Measurements for the Quantitative Determination of Wood Burning and Traffic Emission Contributions to Particulate Matter, Envirn. Sci. Technol., 42, 3316-3323, 10.1021/es702253m, 2008.

Saleh, R., Robinson, E. S., Tkacik, D. S., Ahern, A. T., Liu, S., Aiken, A. C., Sullivan, R. C., Presto, A. A., Dubey, M. K., Yokelson, R. J., Donahue, N. M., and Robinson, A. L.: Brownness of organics in aerosols from biomass burning linked to their black carbon content, Nat. Geosci., 7, 647-650, 10.1038/ngeo2220, 2014.

588 Satish, R., Shamjad, P., Thamban, N., Tripathi, S., and Rastogi, N.: Temporal characteristics of
589 brown carbon over the central Indo-Gangetic Plain, Environ. Sci. Technol., 51, 6765-6772,
590 10.1021/acs.est.7b00734, 2017.
591 Sullivan, A. P., Hodas, N., Turpin, B. J., Skog, K., Keutsch, F. N., Gilardoni, S., Paglione, M.,
592 Rinaldi, M., Decesari, S., Facchini, M. C., Poulain, L., Herrmann, H., Wiedensohler, A., Nemitz,
593 E., Twigg, M. M., and Collett Jr, J. L.: Evidence for ambient dark aqueous SOA formation in the
594 Po Valley, Italy, Atmos. Chem. Phys., 16, 8095-8108, 10.5194/acp-16-8095-2016, 2016.
595 Turpin, B. J. and Huntzicker, J.: Identification of secondary organic aerosol episodes and
596 quantitation of frimary and secondary organic aerosol concentrations during SCAQS, Atmos.
597 Environ., 29, 3527-3544, 1995.
598 U.S.EPA: Review of sunset organic and elemental carbon (OC and EC) measurements during
599 EPA's sunset carbon evaluation project, prepared by Sonoma Technology, Inc., CA 94954-6515,
600 prepared for U.S. Environmental Protection Agency, NC 27711, 2019.
601 Wang, J., Nie, W., Cheng, Y., Shen, Y., Chi, X., Wang, J., Huang, X., Xie, Y., Sun, P., Xu, Z., Qi,
602 X., Su, H., and Ding, A.: Light absorption of brown carbon in eastern China based on 3-year multi-
603 wavelength aerosol optical property observations and an improved absorption Ångström exponent
604 segregation method, Atmos. Chem. Phys., 18, 9061-9074, 10.5194/acp-18-9061-2018, 2018.
605 Wang, P., Cao, J. J., Shen, Z. X., Han, Y. M., Lee, S. C., Huang, Y., Zhu, C. S., Wang, Q. Y., Xu,
606 H. M., and Huang, R. J.: Spatial and seasonal variations of $PM_{2.5}$ mass and species during 2010 in
607 Xi'an, China, Sci. Total. Environ., 508, 477-487, 10.1016/j.scitotenv.2014.11.007, 2015.
608 Wang, Y., Hopke, P. K., Rattigan, O. V., Xia, X., Chalupa, D. C., and Utell, M. J.: Characterization
609 of residential wood combustion particles using the two-wavelength aethalometer, Environ. Sci.
610 Technol., 45, 7387-7393, 10.1021/es2013984, 2011.
611 Wang, Y., Hopke, P. K., and Rattigan, O. V.: A new indicator of fireworks emissions in Rochester,
612 New York, Environ. Monit. Assess., 184, 7293-7297, 10.1007/s10661-011-2497-5, 2012a.
613 Wang, Y., Hopke, P. K., Rattigan, O. V., Chalupa, D. C., and Utell, M. J.: Multiple-year black
614 carbon measurements and source apportionment using delta-C in Rochester, New York, J. Air
615 Waste Manag. Assoc., 62, 880-887, 10.1080/10962247.2012.671792, 2012b.
616 Wu, C. and Yu, J. Z.: Determination of primary combustion source organic carbon-to-elemental
617 carbon (OC/EC) ratio using ambient OC and EC measurements: secondary OC-EC correlation
618 minimization method, Atmos. Chem. Phys., 16, 5453-5465, 10.5194/acp-16-5453-2016, 2016.

Wu, G., Wan, X., Gao, S., Fu, P., Yin, Y., Li, G., Zhang, G., Kang, S., Ram, K., and Cong, Z.: Humic-Like Substances (HULIS) in Aerosols of Central Tibetan Plateau (Nam Co, 4730 m asl): Abundance, Light Absorption Properties, and Sources, Environ. Sci. Technol., 52, 7203-7211, 10.1021/acs.est.8b01251, 2018.

Wu, G., Ram, K., Fu, P., Wang, W., Zhang, Y., Liu, X., Stone, E. A., Pradhan, B. B., Dangol, P. M., Panday, A. K., Wan, X., Bai, Z., Kang, S., Zhang, Q., and Cong, Z.: Water-Soluble Brown Carbon in Atmospheric Aerosols from Godavari (Nepal), a Regional Representative of South Asia, Environ. Sci. Technol., 53, 3471-3479, 10.1021/acs.est.9b00596, 2019.

Wu, G., Wan, X., Ram, K., Li, P., Liu, B., Yin, Y., Fu, P., Loewen, M., Gao, S., Kang, S., Kawamura, K., Wang, Y., and Cong, Z.: Light absorption, fluorescence properties and sources of brown carbon aerosols in the Southeast Tibetan Plateau, Environ. Pollut., 257, 113616, 10.1016/j.envpol.2019.113616, 2020.

Xu, X. and Akhtar, U. S.: Identification of potential regional sources of atmospheric total gaseous mercury in Windsor, Ontario, Canada using hybrid receptor modeling, Atmos. Chem. Phys., 10, 7073-7083, 10.5194/acp-10-7073-2010, 2010.

Yan, C., Zheng, M., Bosch, C., Andersson, A., Desyaterik, Y., Sullivan, A. P., Collett, J. L., Zhao, B., Wang, S., He, K., and Gustafsson, O.: Important fossil source contribution to brown carbon in Beijing during winter, Sci. Rep., 7, 10.1038/srep43182, 2017.

Yan, C., Zheng, M., Shen, G., Cheng, Y., Ma, S., Sun, J., Cui, M., Zhang, F., Han, Y., and Chen, Y.: Characterization of carbon fractions in carbonaceous aerosols from typical fossil fuel combustion sources, Fuel, 254, 10.1016/j.fuel.2019.115620, 2019.

Yang, F., Tan, J., Zhao, Q., Du, Z., He, K., Ma, Y., Duan, F., Chen, G., and Zhao, Q.: Characteristics of $PM_{2.5}$ speciation in representative megacities and across China, Atmos. Chem. Phys., 11, 5207-5219, 10.5194/acp-11-5207-2011, 2011.

Zhang, Q., Shen, Z., Zhang, L., Zeng, Y., Ning, Z., Zhang, T., Lei, Y., Wang, Q., Li, G., Sun, J., Westerdahl, D., Xu, H., and Cao, J.: Investigation of primary and secondary particulate brown carbon in two Chinese cities of Xi'an and Hong Kong in wintertime, Environ. Sci. Technol., 54, 3803-3813, 10.1021/acs.est.9b05332, 2020.

Zhang, W. and Zhang, Y.: Oxygen isotope anomaly ($\Delta^{17}O$) in atmospheric nitrate: a review, Chinese Sci. Bull., 64, 649-662, 10.1360/n972018-01028, 2019.

Zhang, W., Zhang, Y.-L., Cao, F., Xiang, Y., Zhang, Y., Bao, M., Liu, X., and Lin, Y.-C.: High time-

650 resolved measurement of stable carbon isotope composition in water-soluble organic aerosols:
651 method optimization and a case study during winter haze in eastern China, Atmos. Chem. Phys.,
652 19, 11071-11087, 10.5194/acp-19-11071-2019, 2019.
653 Zhang, X., Lin, Y.-H., Surratt, J. D., Zotter, P., Prevot, A. S. H., and Weber, R. J.: Light-absorbing
654 soluble organic aerosol in Los Angeles and Atlanta: a contrast in secondary organic aerosol,
655 Geophys. Res. Lett., 38, 10.1029/2011gl049385, 2011.
656 Zhang, Y. and Kang, S.: Characteristics of carbonaceous aerosols analyzed using a
657 multiwavelength thermal/optical carbon analyzer: a case study in Lanzhou City, Sci. China Earth
658 Sci., 62, 389-402, 10.1007/s11430-017-9245-9, 2019.
659 Zhang, Y., Ren, H., Sun, Y., Cao, F., Chang, Y., Liu, S., Lee, X., Agrios, K., Kawamura, K., Liu,
660 D., Ren, L., Du, W., Wang, Z., Prevot, A. S. H., Szida, S., and Fu, P.: High contribution of nonfossil
661 sources to submicrometer organic aerosols in Beijing, China, Environ. Sci. Technol., 51, 7842-
662 7852, 10.1021/acs.est.7b01517, 2017.
663 Zhang, Y.-L. and Cao, F.: Is it time to tackle $PM_{2.5}$ air pollutions in China from biomass-burning
664 emissions?, Environ. Pollut., 202, 217-219, 10.1016/j.envpol.2015.02.005, 2015a.
665 Zhang, Y. L. and Cao, F.: Fine particulate matter ($PM_{2.5}$) in China at a city level, Sci. Rep., 5,
666 14884, 10.1038/srep14884, 2015b.
667 Zhou, S., Wang, T., Wang, Z., Li, W., Xu, Z., Wang, X., Yuan, C., Poon, C. N., Louie, P. K. K.,
668 Luk, C. W. Y., and Wang, W.: Photochemical evolution of organic aerosols observed in urban
669 plumes from Hong Kong and the Pearl River Delta of China, Atmos. Environ., 88, 219-229,
670 10.1016/j.atmosenv.2014.01.032, 2014.
671 Zhu, C. S., Cao, J. J., Tsai, C. J., Shen, Z. X., Han, Y. M., Liu, S. X., and Zhao, Z. Z.: Comparison
672 and implications of $PM_{2.5}$ carbon fractions in different environments, Sci. Total. Environ., 466-
673 467, 203-209, 10.1016/j.scitotenv.2013.07.029, 2014.

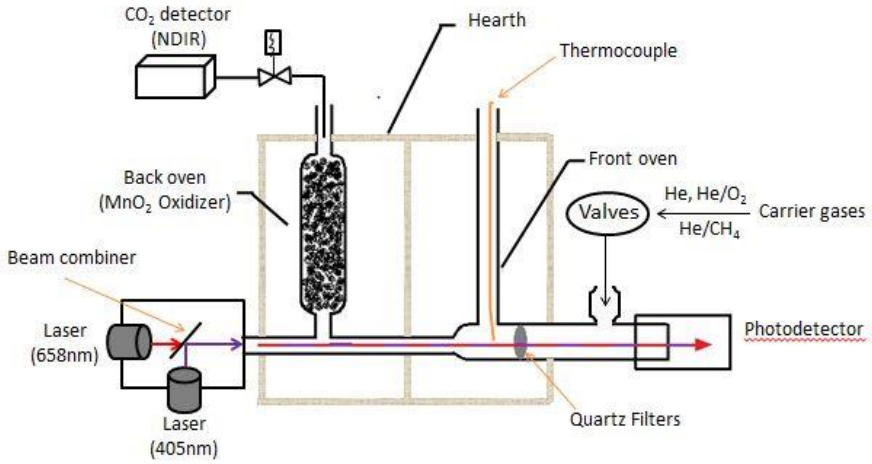

674

675 **Figure 1**. Principle and structure of the Sunset semi-continuous carbon analyzer.

676

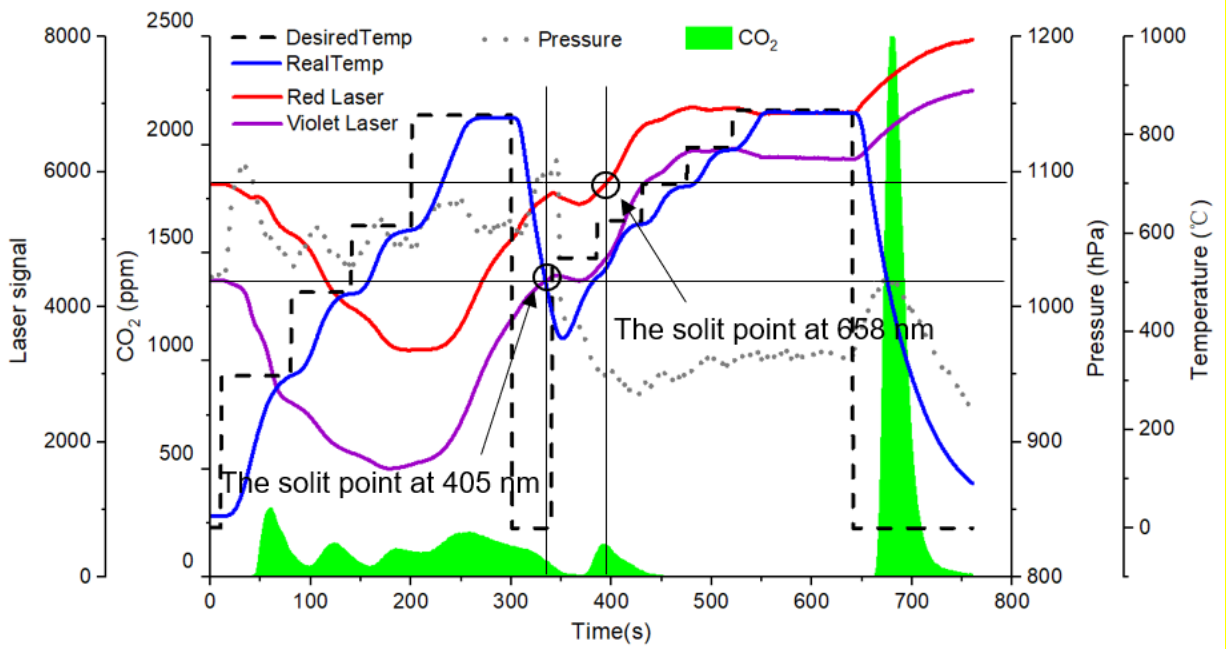

677

678 **Figure 2.** Example thermogram of sample analysis using the two-wavelength Sunset semi-
679 continuous carbon analyzer.

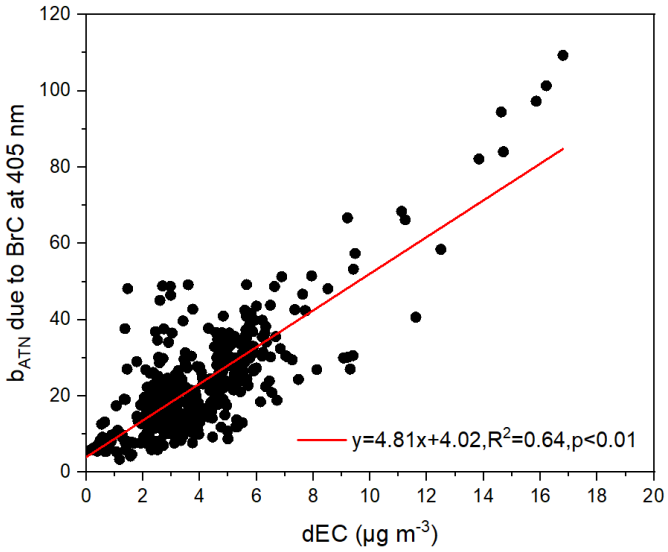

680

681 **Figure 3.** Relationship between the b_{ATN} due to BrC at 405 nm and the dEC concentrations.

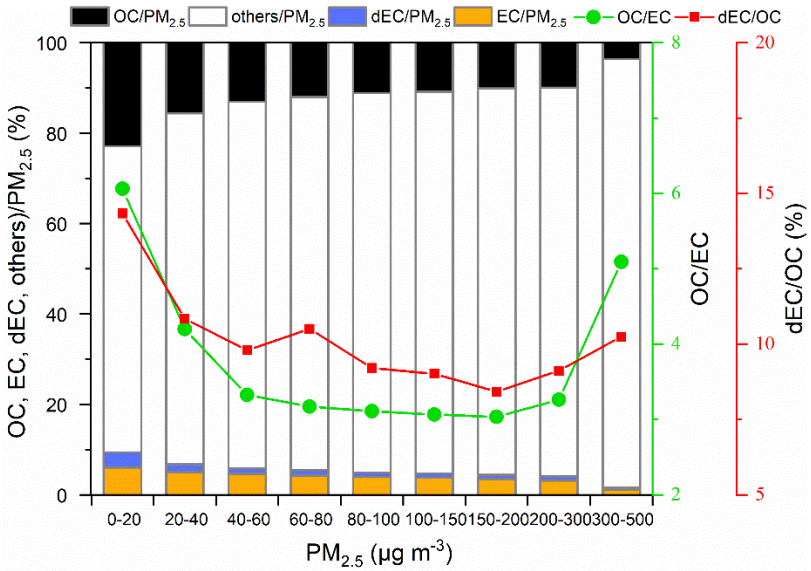

682
683 **Figure 4**. Carbonaceous species fractions of $PM_{2.5}$ and OC/EC ratios at different $PM_{2.5}$
684 concentration intervals at NUIST from June 2015 to August 2016.

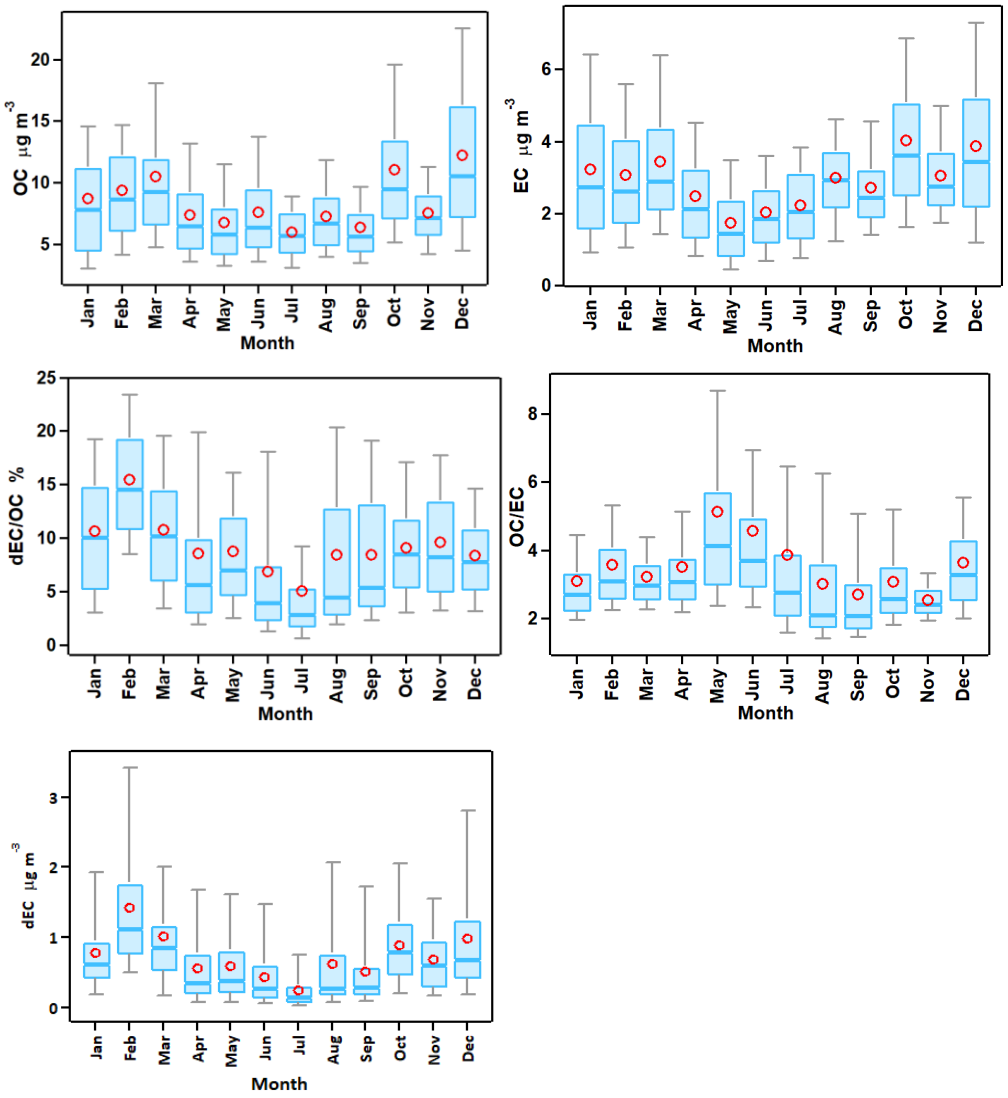

Figure 5. Monthly variations of OC, EC, dEC, dEC/OC and OC/EC ratios at NUIST from June 2015 to August 2016. The boundary of the box indicates the 25% and 75% percentile, respectively. The lower and upper whiskers indicate the 10% and 90% percentile, respectively. The red circle within the box marks the average while the line within the box marks the median.

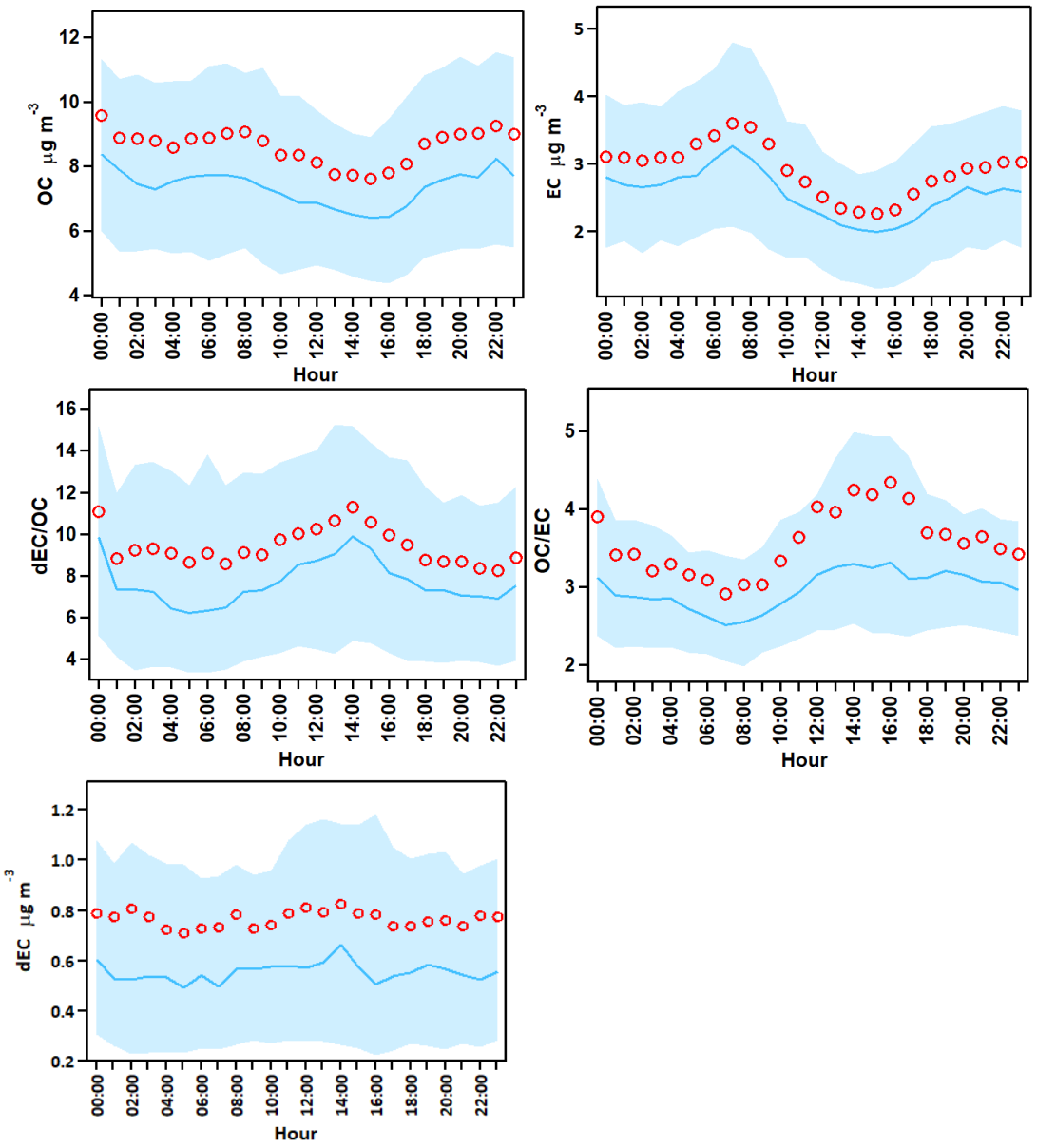

Figure 6. Diurnal variations of OC, EC, dEC concentrations, dEC/OC and OC/EC ratios during the study period. The boundary of the shaded area indicates the 25% and 75% percentile, respectively. The red circle marks the average while the blue line marks the median.

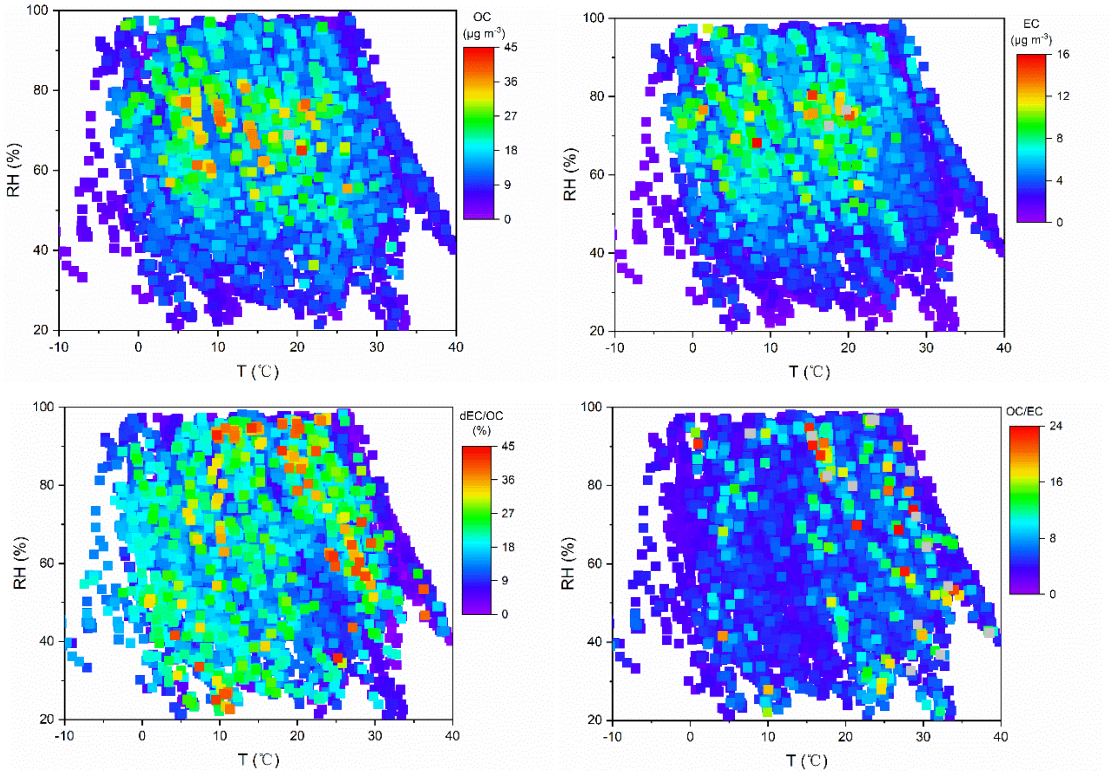

698

699

700 **Figure 7.** RH/T dependence of OC, EC, dEC/OC and OC/EC ratios during the study periods.

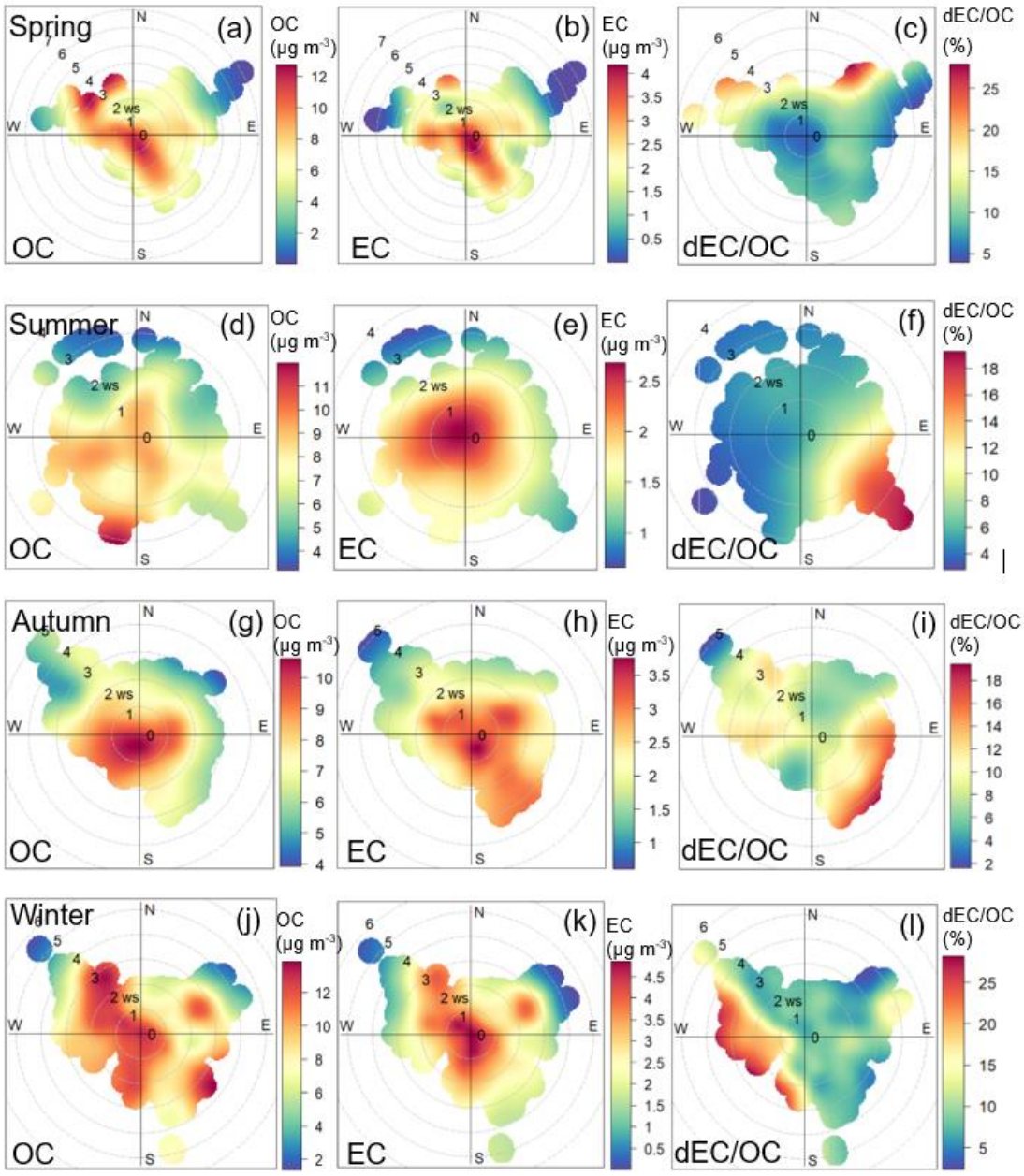

Figure 8. Wind rose of OC, EC and dEC/OC in spring ((a), (b), (c)), summer ((d), (e), (f)), autumn (g), (h), (i)) and winter ((j), (k), (l)).

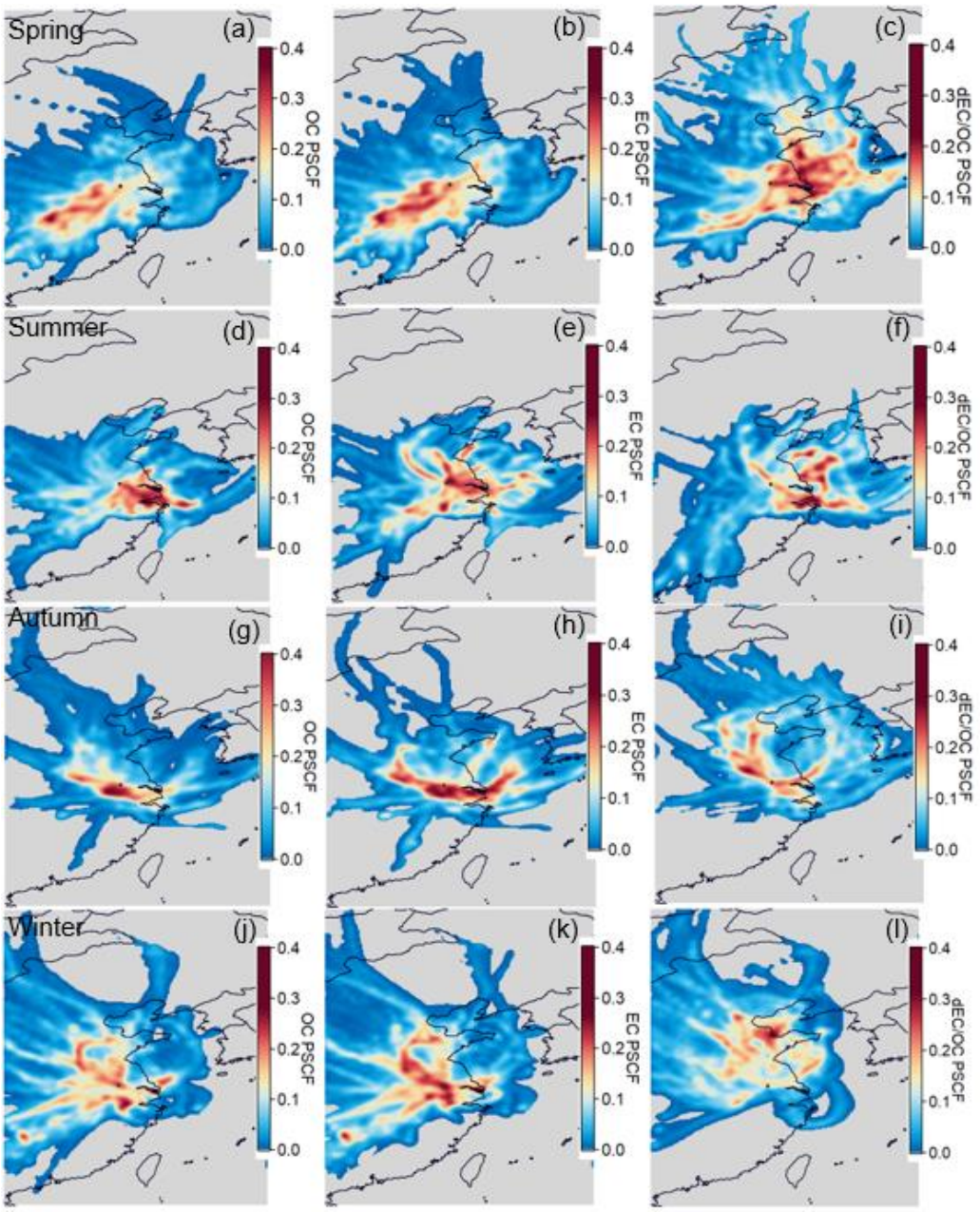

704
705 **Figure 9.** PSCF map for OC, EC and dEC/OC in spring ((a), (b), (c)), summer ((d), (e), (f)), autumn
706 (g), (h), (i)) and winter ((j), (k), (l)).

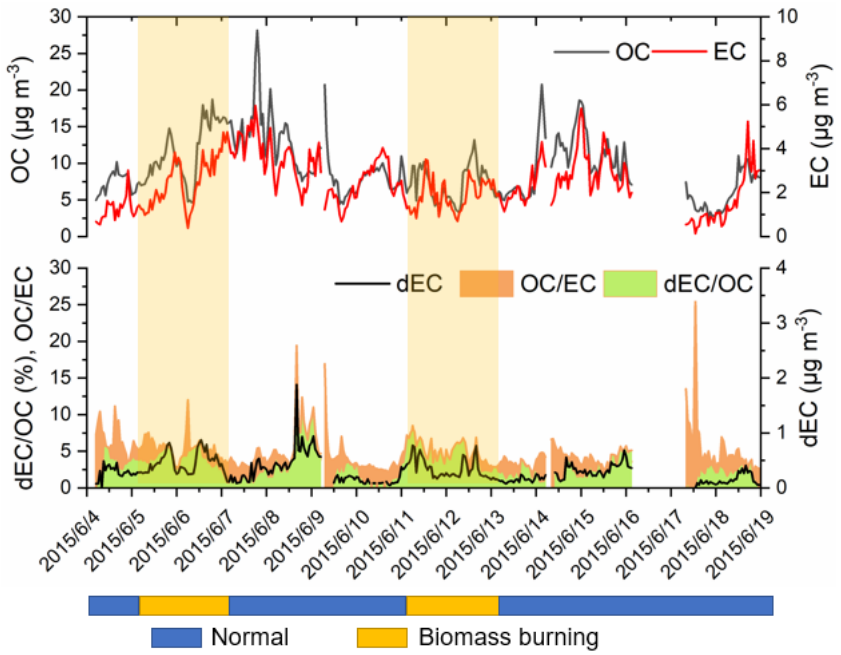

Figure 10. Time series of OC, EC, dEC/OC, dEC and OC/ EC from 4 June 2015 to 19 June 2015. The period was divided into normal days (blue bar) and biomass burning days (yellow bar). The yellow shadow represents the biomass burning periods.

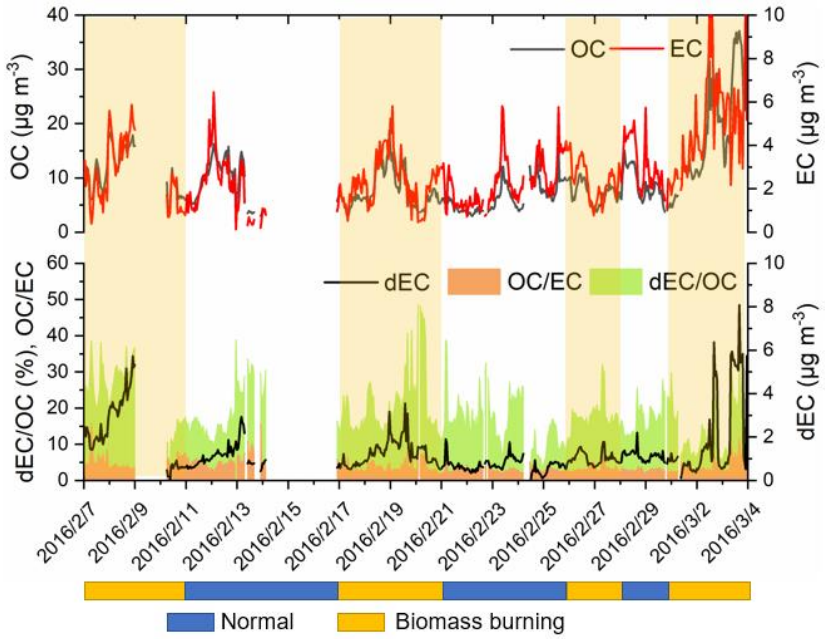

711

712 **Figure 11.** Time series of OC, EC, dEC/OC, dEC and OC/ EC from 7 February 2016 to 3 Mar

713 2016. The period was divided into normal days (blue bar) and biomass burning days (yellow bar).

714 The yellow shadow represents the biomass burning periods.

715 **Table 1.** Statistical summary on the $PM_{2.5}$ and carbon species concentrations.

N=5113	Annual					Spring	Summer	Autumn	winter
	Average	Standard Deviation	Median	Min	Max	Average	Average	Average	Average
$PM_{2.5}$ (μg m^{-3})	77.2	48.6	65.0	2.5	458.1	72.1	47.9	70.5	91.8
OC (μg m^{-3})	8.9	5.5	7.5	0.5	45.8	8.4	7.2	8.4	10.2
EC (μg m^{-3})	3.1	2.0	2.6	0.0	17.6	2.6	2.3	3.3	3.4
OC/EC	3.5	2.4	2.9	1.0	29.3	3.9	4.0	2.8	3.4
dEC (μg m^{-3})	0.8	0.8	0.6	0.0	8.1	0.8	0.5	0.7	1.1
dEC/OC (%)	10.0	7.2	8.6	0.0	48.2	9.5	6.9	9.0	11.3
dEC/EC (%)	22.3	16.7	18.5	0.1	97.8	24.5	18.2	18.7	25.9
OC/$PM_{2.5}$ (%)	12.8	5.6	11.6	0.7	66.2	13.2	14.4	14.1	11.1
EC/$PM_{2.5}$ (%)	4.3	2.3	3.9	0.0	33.2	3.9	4.7	5.8	3.7
dEC/$PM_{2.5}$ (%)	1.3	1.2	0.9	0.0	17.6	1.4	1.3	1.2	1.3

716

Table 2. Statistics of OC, EC, OC/EC, dEC and dEC/OC during biomass burning days and normal days. The values represent average±standard deviation.

		OC ($\mu g\ m^{-3}$)	EC ($\mu g\ m^{-3}$)	OC/EC	dEC ($\mu g\ m^{-3}$)	dEC/OC (**%**)
June 4th to 19th	Normal days	9.5±4.5	2.6±1.3	4.3±2.3	0.2±0.1	2.5±1.3
	Biomass burning days	9.0±3.6	2.0±0.9	4.8±1.6	0.4±0.2	4.6±1.4
February 7th to Mar 3rd	Normal days	7.5±3.3	2.5±1.2	3.3±1.3	0.8±0.3	12.7±5.6
	Biomass burning days	11.2±7.2	3.1±1.9	4.0±1.8	1.7±1.4	15.4±7.8